

Emergence of chromatin hierarchical loops from protein disorder and nucleosome asymmetry

Akshay Sridhar^a, Stephen E. Farr^a, Guillem Portella^b, Tamar Schlick^{c,d,e} , Modesto Orozco^{f,g}, and Rosana Collepardo-Guevara^{a,b,h,1} 

^aMaxwell Centre, Cavendish Laboratory, University of Cambridge, CB3 0HE Cambridge, United Kingdom; ^bChemistry Department, University of Cambridge, CB2 1EW Cambridge, United Kingdom; ^cDepartment of Chemistry, New York University, New York, NY 10003; ^dCourant Institute of Mathematical Sciences, New York University, New York, NY 10012; ^eNew York University–East China Normal University Center for Computational Chemistry, New York University, 200062 Shanghai, China; ^fInstitute for Research in Biomedicine, The Barcelona Institute of Science and Technology, 08028 Barcelona, Spain; ^gDepartment of Biochemistry and Biomedicine, University of Barcelona, 08028 Barcelona, Spain; and ^hDepartment of Genetics, University of Cambridge, CB2 3EH Cambridge, United Kingdom

Edited by José N. Onuchic, Rice University, Houston, TX, and approved February 13, 2020 (received for review June 12, 2019)

Protein flexibility and disorder is emerging as a crucial modulator of chromatin structure. Histone tail disorder enables transient binding of different molecules to the nucleosomes, thereby promoting heterogeneous and dynamic internucleosome interactions and making possible recruitment of a wide-range of regulatory and remodeling proteins. On the basis of extensive multiscale modeling we reveal the importance of linker histone H1 protein disorder for chromatin hierarchical looping. Our multiscale approach bridges microsecond-long bias-exchange metadynamics molecular dynamics simulations of atomistic 211-bp nucleosomes with coarse-grained Monte Carlo simulations of 100-nucleosome systems. We show that the long C-terminal domain (CTD) of H1—a ubiquitous nucleosome-binding protein—remains disordered when bound to the nucleosome. Notably, such CTD disorder leads to an asymmetric and dynamical nucleosome conformation that promotes chromatin structural flexibility and establishes long-range hierarchical loops. Furthermore, the degree of condensation and flexibility of H1 can be fine-tuned, explaining chromosomal differences of interphase versus metaphase states that correspond to partial and hyperphosphorylated H1, respectively. This important role of H1 protein disorder in large-scale chromatin organization has a wide range of biological implications.

H1-nucleosome binding | CTD of H1 | protein disorder | chromatin polymorphism | nucleosome asymmetry

Inside eukaryotic cells, hundreds of millions of DNA base pairs are densely packed inside micrometer-sized nuclei through the formation of a remarkable structure known as chromatin. Chromatin consists of a chain of nucleosomes—nucleoprotein complexes in which the DNA makes ~1.75 turns around a histone protein octamer core (two copies each of H2A, H2B, H3, and H4) (1). Successive nucleosomes are then joined together by linker DNA segments of varying lengths (~10 to 90 bp), making an array termed the 10-nm beads-on-a-string fiber (2). The structure of chromatin beyond the 10-nm fiber remains controversial (2). Evidence for chromatin folding into rigid and straight 30-nm fibers, where nucleosomes interact mainly with their first or second nearest linear neighbors (3, 4), has been obtained primarily for *in vitro* chromatin (5–8). Such chromatin has been reconstituted using uniform DNA positioning sequences, regular nucleosome spacing, and homogeneous histone protein compositions and has often been studied at low ionic strength conditions where neighboring internucleosome interactions are favored (9). However, accumulating evidence suggests that, rather than straight fibers, chromatin *in vivo* can form loops of zigzag nucleosome chains (10–13) and highly dynamic arrangements (14) of irregularly folded 10-nm fibers (15–17) termed liquid-like (9, 16, 18) chromatin elements. Such a flexible chromatin structure *in vivo* agrees with chromatin's heterogeneous characteristics [e.g., non-uniform DNA sequences, irregular nucleosome spacing (17)], and varying histone protein compositions) and other relevant factors

(e.g., nucleosome sliding and eviction, changes in epigenetic marks, and binding of architectural proteins) that impact nucleosome interactions (19). Indeed, recent mesoscale modeling of the 55-kb HOXC gene cluster demonstrated that cooperation among many different chromatin factors, e.g., irregular nucleosome spacing, distribution of acetylation marks, and irregular H1 binding, is crucial for chromatin looping and the formation of functionally relevant long-range chromatin contacts (12).

Nucleosome-nucleosome interactions lie at the center of the chromatin structural puzzle (20). Such interactions are determined by the characteristics of the core histone proteins. Histones are multidomain proteins composed of a relatively rigid globular domain (GD) (1) and positively charged disordered N-terminal tail domains (NTD). The globular regions of the histones, located at the core of the nucleosome, confer their charged and contoured surfaces. Histone tails protrude out of the nucleosome core to serve as highly flexible and sticky arms. Intrinsic disorder allows the tails to sample a region around the nucleosome. Such sampling promotes multiple nonspecific contacts to bridge nucleosome pairs in a multitude of relative orientations and distances, and also

Significance

Inside eukaryotic cells, DNA is organized in the form of chromatin. Protein disorder is abundant both within the chromatin-building blocks—the nucleosomes—and the regulatory chromatin-binding proteins. Such protein disorder facilitates transient and non-specific binding of a wide-range of proteins to the nucleosomes and favors heterogeneity of nucleosome-nucleosome interactions. Here, we reveal additional important roles of protein disorder in chromatin structure regulation: symmetry breaking of the nucleosome-building blocks, enhancement of linker DNA fluctuations, and encouragement of chromatin structural fluidity and long-range regulatory loops. More broadly, our results demonstrate that chromatin-binding proteins can remain disordered or partially disordered when binding to and stabilizing the chromatin fiber.

Author contributions: R.C.-G. designed research; R.C.-G. supervised research; A.S., S.E.F., G.P., and R.C.-G. performed research; A.S., S.E.F., and R.C.-G. analyzed data; and A.S., S.E.F., T.S., M.O., and R.C.-G. wrote the paper.

The authors declare no competing interest.

This article is a PNAS Direct Submission.

Published under the [PNAS license](#).

Data deposition: The atomistic models of H1 containing nucleosomes have been deposited in the University of Cambridge Data Repository (<https://doi.org/10.17863/CAM.49850>).

¹To whom correspondence may be addressed. Email: rc597@cam.ac.uk.

This article contains supporting information online at <https://www.pnas.org/lookup/suppl/doi:10.1073/pnas.1910044117/-DCSupplemental>.

facilitates recruitment of remodeling factors and other chromatin-binding proteins (21, 22).

Linker histones form an additional family of partially disordered histone proteins (23, 24) that have a profound effect on chromatin organization of evolved eukarya (25–29). In vitro, binding of H1 to chromatin stabilizes regular zigzag folding, which has been attributed to the formation of a rigid DNA stem motif with relatively straight DNA linkers (4, 30). Nonetheless, recent electron microscopy tomography data of the ultrastructure of chromatin in intact cells showed that, in vivo, chromatin domains with H1 preserve a flexible and irregular chromatin structure (15).

Among the linker histone family, H1 proteins have a tripartite domain structure: a short NTD [~ 20 to 35 amino acids (AA)], a structured GD also known as the globular head (~ 70 AA), and a long and positively charged C-terminal domain (CTD) (~ 100 AA). Binding of H1 or H5 to the nucleosome results in the formation of a chromatosome particle (31–33). The location of the linker histone within the chromatosome is dictated mainly by the binding of the GD to the nucleosome, which varies across isoforms and with the experimental conditions (6, 32–34). For example, while chicken H5 (33) and *Xenopus laevis* histone H1.0 (34) bind in a symmetric on-dyad mode interacting with both linker DNAs, *Drosophila* H1 (32) and human H1.4 (6) exhibit different types of asymmetric off-dyad binding modes where they interact with only one linker DNA (35). The wide variations in the binding modes of GD suggest that chromatosomes exhibit a heterogeneous ensemble of structures (26, 35). Mesoscale modeling has shown that, in the presence of H1, irregular chromatin folding emerges when the H1 to nucleosome ratio is less than 1:1 (10, 36) and when different on-dyad and off-dyad GD-nucleosome-binding modes are considered (26).

Although the CTD was suggested to exhibit a disorder-to-order transition when binding to DNA (37), more recent studies have shown that the CTD remains highly disordered after binding to either DNA (24) or a negatively charged disordered protein (38). In addition, cryo-Electron Microscopy (cryo-EM) and X-ray crystallography of a 197-bp nucleosome particle with H1 showed preferential and asymmetric interactions of the CTD with one of the DNA linkers and loss of the two-fold nucleosome symmetry (34). Binding of H1 to a full nucleosome with long DNA linkers is expected to impose additional constraints to the CTD. Indeed, fluorescence resonance energy transfer (FRET) experiments demonstrate that the CTD exhibits a different degree of condensation when bound to free DNA, a mononucleosome, or oligonucleosomes (39). Similarly, our previous modeling of oligonucleosomes with H1 revealed the synergistic condensation of CTD and the chromatosome (40). Because of its length and diverse conformational landscape, characterizing the structure of the CTD at atomic resolution when H1 is bound to a nucleosome has not yet been possible. Hence, whether the structural disorder of H1 is preserved or hindered when it is bound to the nucleosome remains unclear.

Here, we develop an advanced multiscale modeling and simulation strategy to characterize the structural behavior of H1 when it binds to the nucleosome and investigate the implications in large-scale chromatin structure. Our methodology exploits the latest experimental structural data of linker histones and chromatosomes (33, 34) and bridges atomistic molecular dynamics (MD) simulations of 211-bp nucleosomes with nucleosome-resolution Monte Carlo (MC) simulations of 100-nucleosome chromatin fibers. We show that, upon binding to a 211-bp nucleosome, the GD of H1 preserves its secondary structure (41) and crystallographic on-dyad binding location (34); the CTD remains unstructured and compact, and the NTD undergoes a disorder-to-order transition. Because of these differences, asymmetric interactions with the two different DNA linkers occur. The resulting imbalance induces the formation of an asymmetric 211-bp nucleosome with DNA linkers that cross each other and bend unevenly.

The implications on fiber structure are profound: long-range loop contacts emerge naturally, forming binding regions for regulatory proteins. That is, increased flexibility of the DNA linkers due to H1 asymmetry increases chromatin structure irregularity and facilitates the formation of linearly distant inter-nucleosome contacts, which are not favored in chromatin with symmetrical and rigid nucleosomes (17). Such behavior is consistent with the hierarchical looping model (10–13) which proposes that 10-nm chromatin fibers are compacted laterally into self-associating loops which then stack and fold in space. The term “hierarchical looping” refers to a polymer that has been compacted laterally without knotting, with loops of various sizes undergoing further folding in space (10–13), not an ordered chromatin structure such as the canonical 30-nm fiber. Moreover, phosphorylation of serines and threonines in the CTD of H1 modulates the ability of chromatin to form long-range hierarchical looping interactions (10–13). While partial phosphorylation leads to chromatin fibers with intermediate flexibility that can form some long-range hierarchical looping interactions (10–13), hyperphosphorylation increases significantly the flexibility, compaction, configurational diversity, and long-range looping interactions of chromatin. Together, our results shed light on a longstanding discussion of the roles and structural behavior of the H1 CTD within the nucleosome particle and chromatin structure.

Multiscale Model. To characterize the statistical ensembles of the nucleosome-bound H1 with atomistic resolution and its implications in chromatin nanoscale structure, we have developed an advanced multiscale methodology that combines two complementary levels of resolution (Fig. 1). At the atomic level, we use the latest experimental structural data available for H1 (33, 34) to build initial models and then perform a set of microsecond-long, enhanced-sampling, explicit-solvent MD simulations of 211-bp nucleosomes with one H1 protein bound (H1.0 variant), truncated nucleosomes with various degrees of H1 phosphorylation, and isolated H1 terminal regions. The 211-bp nucleosomes include two symmetric 32-bp DNA linkers, termed DNA linker $\alpha 3$ and L1 as in ref. 33 (Fig. 1A). To determine the reliance of our results on the underlying forcefield, we compared three different force-field combinations: Amber99SB-ILDN (42) + parmbsc0 (43) + TIP3P (44); Amber03ws (45) + parmbsc0 + TIP4P-2005 (46); and Charmm36M (47) + Charmm36 DNA (48) + TIP3P (*SI Appendix, Table S1*, lists all our atomistic simulations). At the nucleosome-resolution level, we modeled 100-nucleosome systems with one H1 bound to each nucleosome (see Fig. 1B and *SI Appendix, Supporting Methods* for details). We modeled H1.0 (including NTD, GD, and CTD) as a flexible heteropolymer with a resolution of one bead per five amino acids (37 beads) as before (40) but added elastic parameters (i.e., stretching and bending force constants and equilibrium values) derived by Boltzmann inversion of the corresponding equilibrium ensembles for the atomistic nucleosome-bound H1 system from bias-exchange metadynamics (BE-MetaD) (Fig. 1C). The charges for the structured GD beads are optimized to fit the electric field of the atomistic model using the DiSCO algorithm (49), while those for the disordered tails are defined by the total charge of the amino acids that they represent. Our present multiscale (atomistic and coarse-grained) approach can show how H1 remains disordered upon nucleosome binding and what this effect has on entering/exiting DNA linkers. It is also computationally feasible to investigate the implications of such disorder in large-scale chromatin entities.

Results

Nucleosome-Bound H1 Is Highly Disordered. For determining the structural behavior of the nucleosome-bound H1 system at atomistic resolution, we performed BE-MetaD simulations with an accumulated sampling of 25 μ s and repeated with three different force

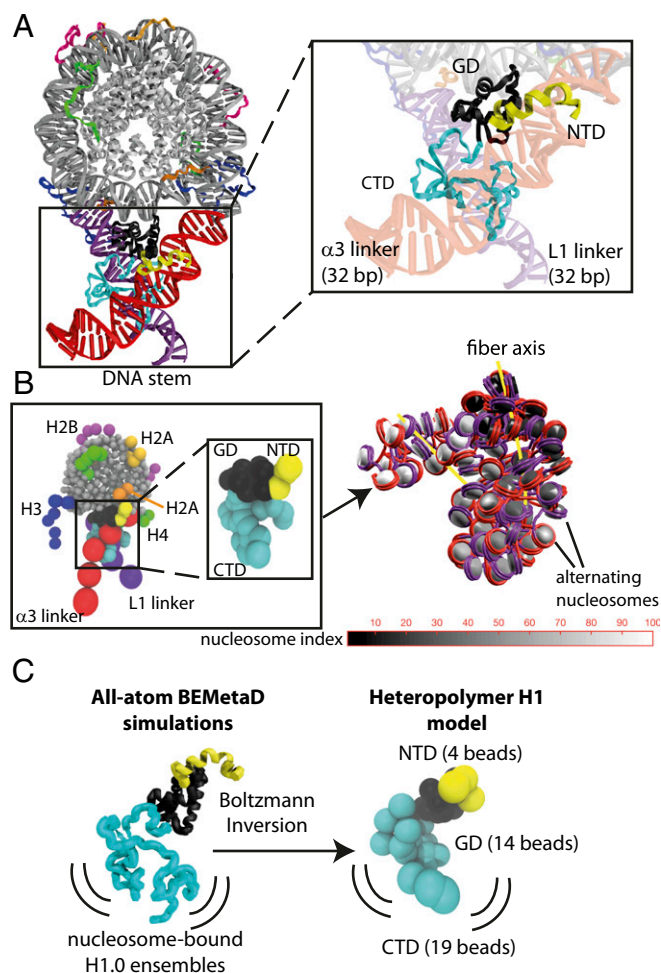


Fig. 1. Illustration of our multiscale methodology. (A) Atomistic model of a 211-bp nucleosome with a full-length human H1.0 bound. The globular, amino, and carboxyl domains are shown in black, cyan, and yellow, respectively. (B) Coarse-grained chromatin model with resolution of five amino acids per bead including the NTD, GD, and CTD and incorporating atomic fluctuations: (Left) detailed bead representation of the model for one nucleosome and (Right) a space-filling representation of a 100-nucleosome system with nucleosomes colored according to their index, DNA on alternating nucleosomes colored red and purple, and fiber axis in yellow (linker histones are not shown in this representation to ease visualization). (C) Multiscale approach developed in this work to parameterize H1 using the equilibrium ensembles from metadynamics MD simulations of the human H1.0 bound to a 211-bp nucleosome in explicit solvent and ions.

fields (see *SI Appendix, Supporting Methods* for details on collective variables and the metadynamics protocol). These simulations reveal that H1 efficiently screens the electrostatic repulsion among the two 32-bp linker DNA arms inducing a “DNA stem”—a motif formed by the two linker DNA arms that cross (Fig. 1A). In contrast, microsecond-long atomistic MD simulations of a 187-bp nucleosome without the H1 show large fluctuations of the DNA linkers and no crossing (50).

Our control 9- μ s long Replica Exchange with Solute Scaling (REST2) simulations of an isolated CTD peptide in solution (see description of REST2 simulations in the *SI Appendix, Supporting Methods*) show that the CTD is more condensed when bound to the nucleosome than when it is free in solution (Fig. 2A), in agreement with experimental observations (51, 52). Yet, despite this higher degree of compaction, the nucleosome-bound CTD remained flexible as shown by broad distributions in the end-to-end distance and radius of gyration (Fig. 2A) and by the root

mean square fluctuation (RMSF) values (Fig. 2B). In fact, both the free CTD in solution and within the nucleosome exhibit mainly disordered conformations with residual beta-fold elements (Fig. 2C), suggesting that, contrary to a previous hypothesis (37), CTD condensation is not the result of a disorder-to-order secondary structure transition. This disordered nature of the

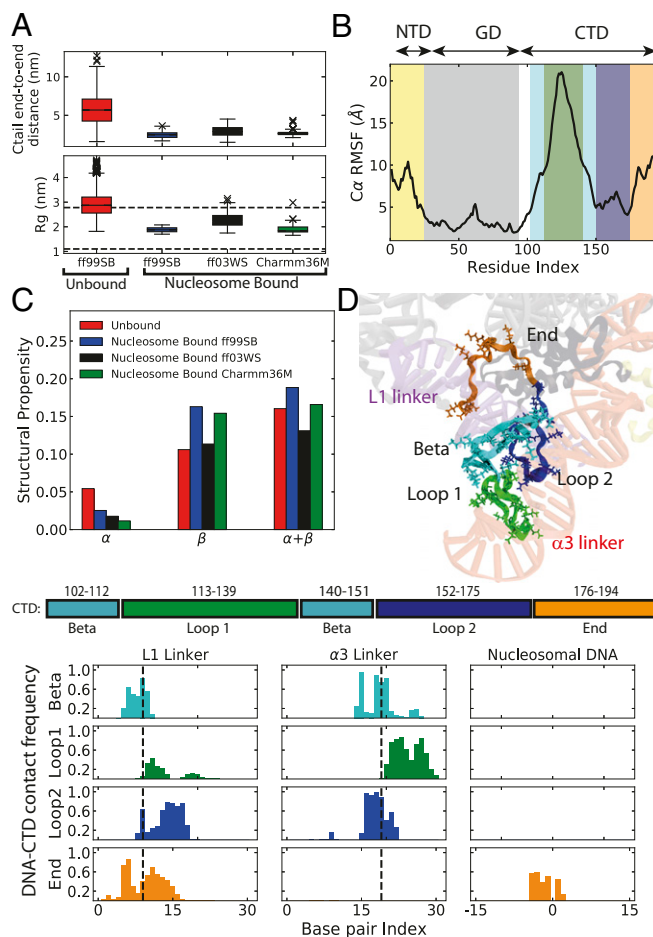


Fig. 2. CTD structure and interactions with DNA within a 211-bp nucleosome. (A) End-to-end distance (Top) and radius of gyration (Bottom) of the CTD Ca atoms comparing simulations for the isolated peptide in solution (Unbound) and for the full H1 bound to the nucleosome (Bound) repeated with three different force fields. For the radius of gyration, the 2.78 and 1.10 nm values predicted from an experimental regression (*SI Appendix, Supporting Methods*) for a 98-residue intrinsically disordered and globular protein, respectively, are shown with dashed lines (64, 65). The data are presented in boxplots. All boxplots in this work show a colored box representing the 25 to 75 percentile range, a line inside the box shows the median, the Notch displays the 95% confidence interval around the median, the whiskers show the region including ~99.3% of the data, and the crosses show outliers. (B) RMSF fluctuations of the nucleosome-bound H1 Ca atoms versus the residue index calculated from the neutral replica of the BE-MetaD simulations. The NTD and GD residues are shaded yellow and gray, respectively. The CTD residues are shaded according to the lysine-rich loop region they belong to (see color coding in D). (C) Secondary structural content from simulations of the CTD in the unbound and nucleosome-bound states for three different force fields show that the CTD remains mostly disordered. (D) Partitioning of CTD into four loop regions, all disordered except one, that interact differentially with the two linker and nucleosomal DNAs. A structure of the CTD within the most populated cluster of the simulation is shown with the four loop regions colored as follows: Beta in cyan, Loop 1 in green, Loop 2 in blue, and End in orange. Lysine residues are shown with sticks for emphasis. The bar plots show the frequency of DNA-CTD contacts between the four CTD regions and the DNA ($\alpha 3$ DNA linker, L1 DNA linker, and nucleosomal DNA).

nucleosome-bound H1 CTD emerges independently of the force field used (Fig. 2C). Despite their overall disorder, the statistical ensembles stemming from our BE-MetaD simulations reveal that the CTD can be partitioned into four different structural regions that exhibit distinct patterns of interactions with the DNA in the nucleosome (Fig. 2D, *SI Appendix*, Fig. S1, and detailed description in *SI Appendix*, *Supporting Methods*). In contrast, the short NTD adopted a significant helical population upon DNA binding (*SI Appendix*, Fig. S2), and the GD preserved its winged-helix fold throughout the simulations (*SI Appendix*, Fig. S3A)

H1 Binding Breaks the Symmetry of the Nucleosome. A common feature observed for all force fields is that the DNA stem has an asymmetric conformation formed by two curved DNA arms that crisscross the nucleosome dyad axis at uneven base-pair positions (Fig. 3A and *SI Appendix*, Fig. S4). This asymmetry is consistent with our previous modeling work (26, 40) as well as with recent cryo-EM and an X-ray crystallography study of a 197-bp nucleosome particle with H1 showing preferential and asymmetric interactions of the CTD with one of the DNA linkers and loss of the two-fold nucleosome symmetry (34). The presence of the H1 tail domains is necessary for the formation of the asymmetric and compact DNA stem. Indeed, our control unbiased MD simulations of 211-bp nucleosomes with only the H1.0 GD show DNA linkers that approach each other symmetrically (*SI Appendix*, Fig. S4).

The flexibility of the linker DNA impacts strongly the possible nucleosome-nucleosome arrangements within condensed chromatin (4). The size of the fluctuations of the DNA linkers in the stem increases significantly after the DNA-DNA crossing point (Fig. 3B). In addition, in the region between the nucleosome edge and the DNA-DNA crossing point, binding to the disordered CTD increases the flexibility of the DNA linkers with respect to binding to the GD only (Fig. 3B). This is because before the crossing-point DNA linkers interact strongly with both the rigid

GD and the flexible CTD, but beyond the crossing point, they interact exclusively with the flexible CTD (Fig. 3C and D).

Prior mesoscale modeling revealed that straight and ordered 30-nm zigzag fibers are favored when the DNA linkers adopt symmetric and rigid stem conformations (4, 17). Moreover, our studies have shown that conditions yielding uneven DNA stems and, hence, irregular DNA bending—such as nonuniform nucleosome spacing (17), nucleosome eviction (17), H1-to-nucleosome ratios lower than 1:1 (10, 12, 36), or low salt (40)—promote instead irregular folding of the 10-nm fibers (e.g., loops, hairpins, and bends) (17) and hierarchical looping (10–13). These findings agree with the organization of chromatin proposed based on cryo-EM images of mitotic chromosomes, in which irregular structures are predominant and 30-nm fibers can form (53). Our present atomistic simulations show that the nucleosome-bound H1 also adopts asymmetrical configurations. The H1 asymmetry leads to a higher degree of bending exhibited by the $\alpha 3$ versus the L1 DNA linkers (dimensionless DNA helical axis curvature is 1.13 for $\alpha 3$ but only 0.78 for L1; *SI Appendix*, *Supporting Methods*) and results in the DNA-DNA crossing point occurring at uneven positions in the $\alpha 3$ versus L1 DNA linkers (i.e., base pair 19 of linker $\alpha 3$ and base pair 9 of linker L1; Fig. 3A).

To further rationalize the molecular origin of the nucleosome asymmetry, we computed the frequencies of interactions between the three different H1 domains and the nucleosomal $\alpha 3$ linker and L1 linker DNA regions (Fig. 3D; *SI Appendix*, Fig. S1). We found that the observed asymmetry correlates with uneven CTD-DNA electrostatic interactions. Because of its short length and being fixed by the rigid globular head to face the $\alpha 3$ DNA linker, the H1.0 NTD (carrying six positively charged residues) is limited to interact exclusively with the first few base pairs (5 to 15 bp) of the $\alpha 3$ linker DNA (Fig. 3D). As observed experimentally (32), the GD interacts most strongly with the nucleosomal DNA and asymmetrically with the first ~ 10 bp of the L1 and $\alpha 3$ DNA linkers. The disordered CTD—carrying 42 positively

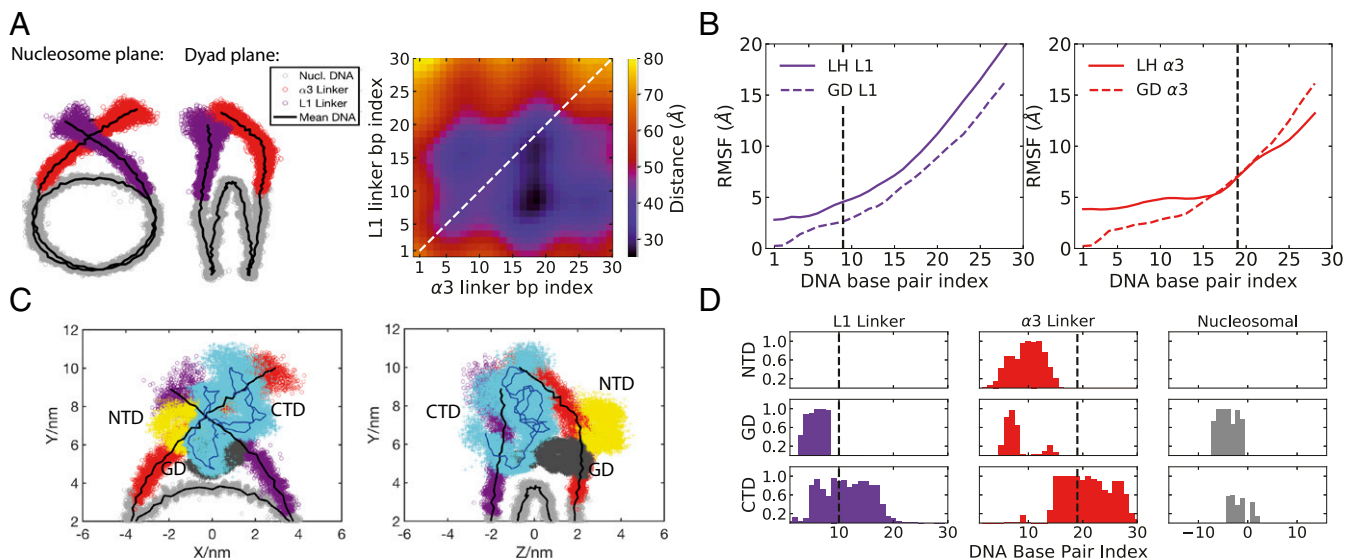


Fig. 3. Two-fold symmetry breaking of the nucleosome upon H1 binding. (A) Formation of an asymmetric conformation of the linker DNA arms from BE-MetaD simulation with full-length H1 depicted through a nucleosomal (*Left*) and dyad (*Right*) planes. The $\alpha 3$ and L1 linkers are shown in red and purple, respectively, and the nucleosomal DNA in gray. This asymmetry is evident from the per-base-pair interlinker strand distance matrix shown. For comparison, the formation of a symmetrical nucleosome from simulations with only the H1 globular head is shown in *SI Appendix*, Fig. S4. (B) RMSF values for the two DNA linkers (linker L1: *Left*; linker $\alpha 3$: *Right*) versus DNA base-pair index. The DNA-DNA crossing point is shown with a dashed line. The differences in RMSF reveal smaller fluctuations before the DNA-DNA crossing point due to interactions with the rigid GD and higher fluctuations thereafter. (C) Uneven interactions between the H1 domains and the two linker DNA arms highlighted through the projection of the BE-MetaD trajectory on the nucleosomal (*Left*) and dyad (*Right*). The $\alpha 3$ and L1 linkers are shown in red and purple, respectively; the nucleosomal DNA in gray; and the amino, globular, and carboxyl domains of H1.0 are shown in yellow, gray, and cyan, respectively. (D) The uneven patterns of H1-DNA interactions for the three H1 domains and the DNA regions in the stem. A contact was assumed if a nonhydrogen atom of the base pair was within 3.4 Å of a nonhydrogen H1 atom.

charged residues (55% of its total residues)—acts as an imbalanced bridge between the two DNA linkers (see also *SI Appendix, Fig. S3B*). It interacts strongly with the first ~23 bp of the L1 linker DNA and then with the last ~15 bp of the more curved and flexible $\alpha 3$ linker DNA. Consistently, the CTD has been shown to interact preferentially with the L1 linker in a nucleosome with 25-bp DNA linkers (34) and with the $\alpha 3$ linker after the DNA-DNA crossing point and up to base pair 30 (51).

Both the symmetry break of the nucleosome and the ability of the linker DNA to fluctuate notably beyond the crossing point are highly significant as they paint a dynamical and irregular picture of the DNA stem—a building block for the more fluid organization of nucleosomes within compact chromatin (16).

A Coarse-Grained Model Designed to Capture CTD Heterogeneity and Disorder Predicts a Flexible Structure of Chromatin at the Nanoscale.

Having characterized the atomistic behavior of the 211-bp nucleosome with one H1 protein bound to it, we next investigated how our observations impact nanoscale chromatin structure. To account for the flexible CTD, we incorporated into our meso-scale chromatin model H1 protein parameters by Boltzmann inversion of the atomistic bond and angle distributions (*SI Appendix, Supporting Methods and Figs. S5 and S6*). These parameters yielded a nonuniform elastic force field for the CTD (heteropolymer model). We sampled configurations of 100-nucleosome chromatin fibers with one H1 molecule bound to each nucleosome and a nucleosome repeat length of 200 bp (using 12 MC trajectories per simulated system that explore four random seeds and three DNA twist deviations around the mean to mimic natural variations). We also investigated how the CTD model affected our predictions by repeating simulations with a less flexible (LessFlex) and more flexible version (MoreFlex) of our heteropolymer CTD model and with a uniform elastic force field that forces the CTD to adopt a symmetric configuration (Symmetric) (see description in *SI Appendix, Supporting Methods*). Fig. 4A shows the differences in CTD end-to-end distances and radii of gyration predicted by the various conditions that we tested. While chromatin *in vivo* is characterized by irregular DNA linker lengths (17) and low H1-to-nucleosome ratios (26), here we model chromatin with uniform linker DNA lengths and 1:1 H1 to nucleosome ratios. These regular chromatin conditions allow us to isolate the effect of H1 disorder in large-scale organization and control for competition and cooperation among different factors. The heterogeneity and asymmetry of the H1 CTD leads to chromatin hierarchical looping (10–13) and polymorphism even for chromatin under regular conditions. That is, when the CTD is flexible and asymmetric within chromatin, regular zigzag folding is destabilized and chromatin instead exhibits significantly wider distributions of the sedimentation coefficients, nucleosome-nucleosome orientations, and chromatin end-to-end distances than those emerging from a symmetric CTD (Fig. 4B and C and *SI Appendix, Fig. S7*). To further characterize the modulation of chromatin flexibility by changes in the behavior of the CTD of H1, we monitored the decay of the tangent-tangent correlation function (*SI Appendix, Fig. S8*). The correlation decays more slowly than exponential decay at short contour lengths and increases as the nucleosome-nucleosome linear separation grows. This suggests that the coupling of the internal chromatin degrees of freedom and the formation/breakage of numerous and highly diverse attractive internucleosome interactions lead to a complex behavior where the local stiffness of chromatin is not well described by the wormlike chain model within the length scales that we can access with our simulations. Note that our chromatin systems are relatively short (~150 to 250 nm; *SI Appendix, Fig. S7*) in comparison with the estimated persistent length of chromatin [~170 to 220 nm (54)]. Still, we observed a faster decay with contour length for the

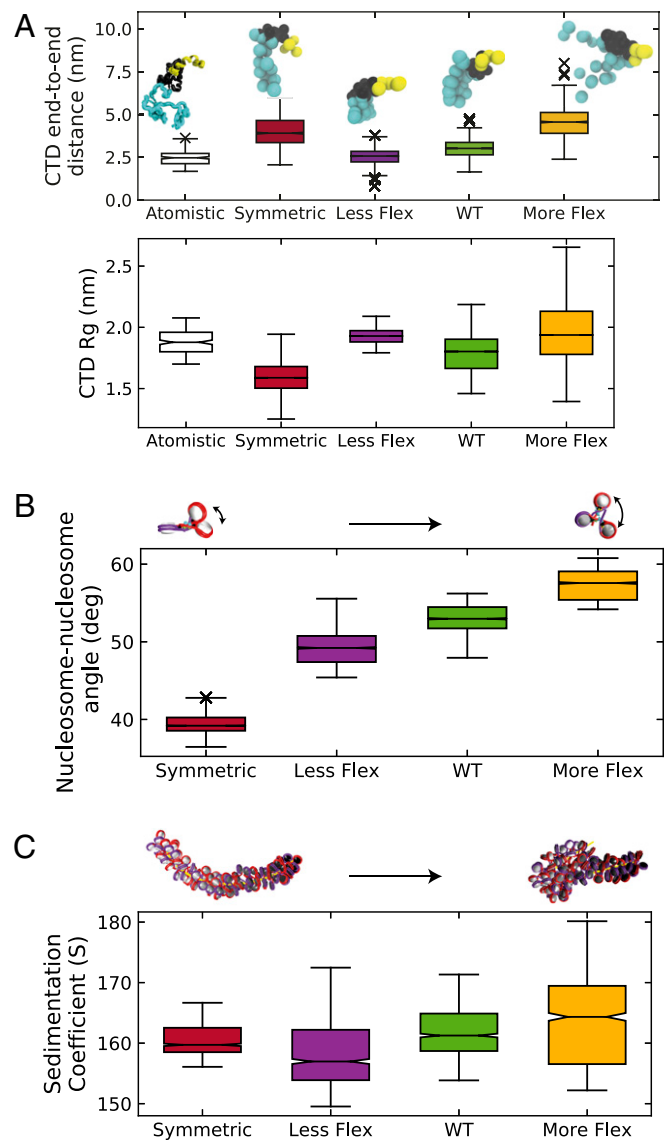


Fig. 4. Impact of the H1 CTD coarse-grained model in the prediction of chromatin nanoscale structure. (A) Comparison of Notch box plots for the CTD end-to-end distances and radii of gyration between the atomistic nucleosome-bound system (ff995B, other force fields shown in Fig. 2) and the coarse-grained model derived in this work (WT) from the atomistic statistical ensembles of the nucleosome-bound H1. We also analyze the effect of imposing instead a symmetric CTD configuration (Symmetric), and of decreasing (Less Flex) or increasing the flexibility of H1 (More flex) (i.e., by multiplying or dividing the bending and stretching constants of the WT model by a factor of 10 for Less Flex and More Flex, respectively). A representative equilibrium configuration for each of the different CTD models is shown inside the plot. (B) Nucleosome-nucleosome triplet angles (defined by the centers of nucleosomes i , $i + 1$, and $i + 2$). (C) Sedimentation coefficients for 100-nucleosome systems with one H1 per nucleosome and varying CTD coarse-grained models. Box plots for the coarse-grained systems were obtained by bootstrapping the results from 12 independent MC trajectories per case.

chromatin systems that exhibit larger fluctuations in their geometrical fiber descriptors, consistent with greater flexibility.

The structural fluidity emerging from H1 CTD disorder is also evident from the high proportion (more than 50% of conformations) of internucleosome contacts between nucleosomes separated by 15 or more neighbors (3 kb) (orange bars in Fig. 5A) that our multiscale approach predicts when the CTD is asymmetric. In comparison, chromatin with a symmetric CTD favors

regular zigzag folding with no long-range contacts (Fig. 5A). Moreover, longer range contacts among nucleosomes separated by 5 kb or more form occasionally for chromatin with an asymmetric CTD, becoming more prominent as the flexibility of the CTD model increases (Fig. 5A). The hierarchical loops and bundles of flexible zigzag nucleosomal chains that enable these long-range contacts (Fig. 5B–D) are similar to those that we observed in a series of recent modeling works for chromatin with irregular compositions (10–13). Our results here thereby propose that H1 disorder and the asymmetry of the nucleosome impact chromatin organization significantly by enhancing long-range contacts (10–13) and by increasing the bending brought about by H1 asymmetric nucleosome binding (26).

Phosphorylation Affects H1 Flexibility and Modulates Chromatin Structure. The family of H1 proteins is highly diverse, including at least 11 subtypes in mammals, which are associated with different functions (55, 56). H1 also contains various sites for posttranslational modifications, with the most common being phosphorylation of serines in the SP(K/A)K motifs and of threonine residues (57). Because we had observed that the electrostatic DNA-CTD contacts and CTD disorder are crucial for the formation of the asymmetric nucleosome conformation, we next investigated how different degrees of serine and threonine phosphorylation affected these results.

For this investigation, we performed additional 5- μ s BE-MetaD simulations of a reduced system in which we truncated part of the nucleosome keeping only the 30 bp of nucleosomal DNA, the two

32-bp DNA linkers, the full H1, and the histone tails H3, H4, and H2AC because of their proximity to the dyad (Fig. 6A). We ran simulations for three cases: wild-type (WT) H1, partial H1 phosphorylation (30% of CTD serine/threonine; *SI Appendix, Fig. S10*), and hyperphosphorylation (all CTD serine/threonine residues). For comparison, we also performed additional REST2 simulations in explicit solvent and ions of the isolated CTD in the partial and hyperphosphorylated states.

We found that the degree of compaction of the unbound CTD increases as the degree of phosphorylation increases (Fig. 6B). This can be readily explained by the increasing number of favorable intraprotein contacts between lysines and phosphorylated residues that stabilize closed conformations. Surprisingly, this monotonic effect of phosphorylation is not maintained when the CTD is bound to the nucleosome. While the nucleosome-bound hyperphosphorylated CTD exhibits a similar distribution of the end-to-end distance as the WT domain (Fig. 6C), the nucleosome-bound partially phosphorylated CTD appears decondensed when compared to the WT case (Fig. 6C). In the partially phosphorylated case, we observed competitive interactions of the lysine residues with the phosphorylated residues and the DNA backbone, which enhanced the dynamic nature of the CTD-DNA binding events (*SI Appendix, Figs. S11 and S12*). In the fully phosphorylated case, the lysine-phosphorylated residue interactions dominate and thereby allow the reverting of the CTD to a condensed state similar to that of the WT.

To explore the implications of the phosphorylated CTD's conformational preferences on large-scale chromatin organization, we

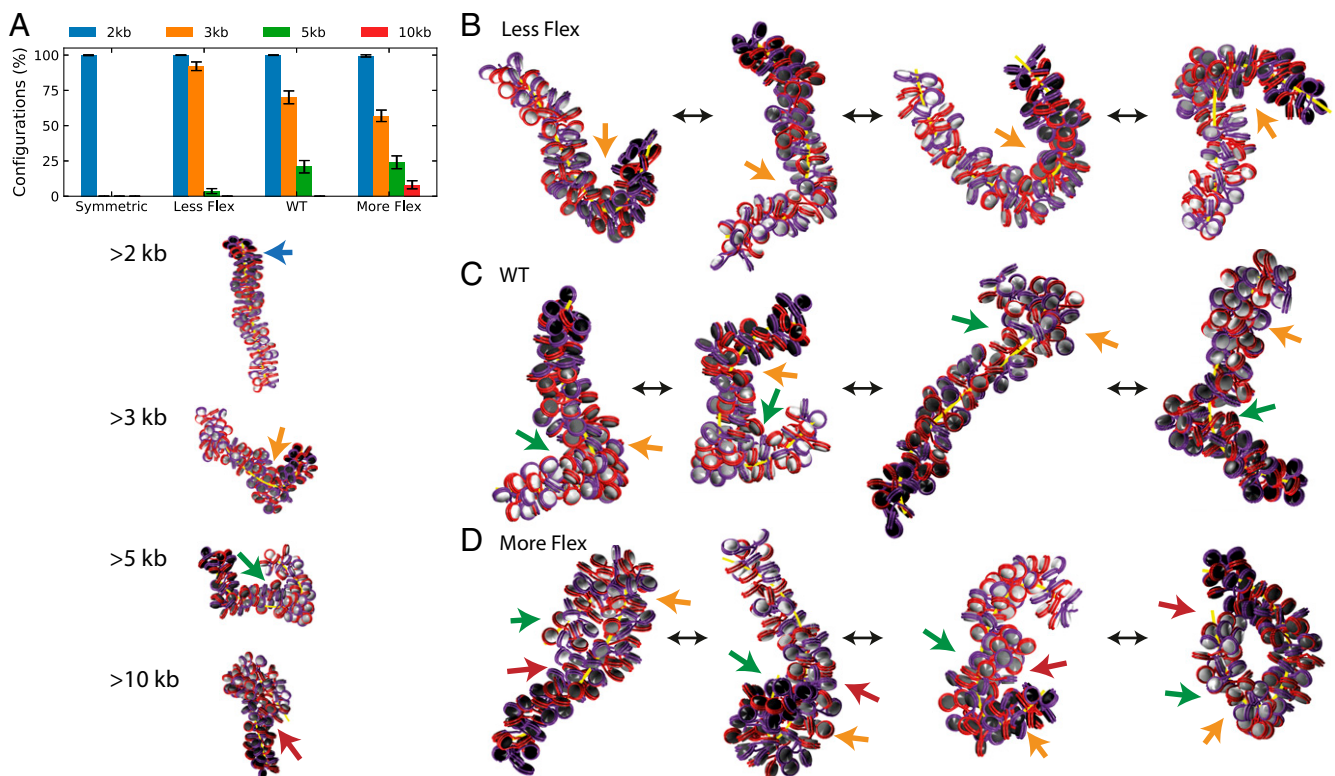


Fig. 5. Impact of the H1 CTD coarse-grained model in the prediction of hierarchical looping. (A) Percentage of configurations with short-range contacts among nucleosomes (blue bars: separated by 2 kb) and long-range contacts (orange, green and red bars: separated by 3, 5, and 10 kb, respectively) with error bars representing 95% confidence intervals obtained by bootstrapping the results from the independent simulations. Examples of structures with different long-range contacts are also shown together with colored arrows (blue, orange, green and red for 2, 3, 5, and 10 kb, respectively) pointing toward the contact region to facilitate visualization. (B–D) Space-filling models illustrating configurations with different long-range contacts for 100-nucleosome systems with one H1 per nucleosome and varying CTD coarse-grained models (color coding in Fig. 1). The 2-kb interactions are not indicated in these images as they are ubiquitous. To further quantify the persistence of the different structures presented, the probability of loop formation as a function of loop size for the different systems is calculated in *SI Appendix, Fig. S9*. These probabilities are distinctly different for each system. The probability of forming increasingly longer loops signals greater chromatin flexibility and is positively correlated with the flexibility of the CTD H1 model used.

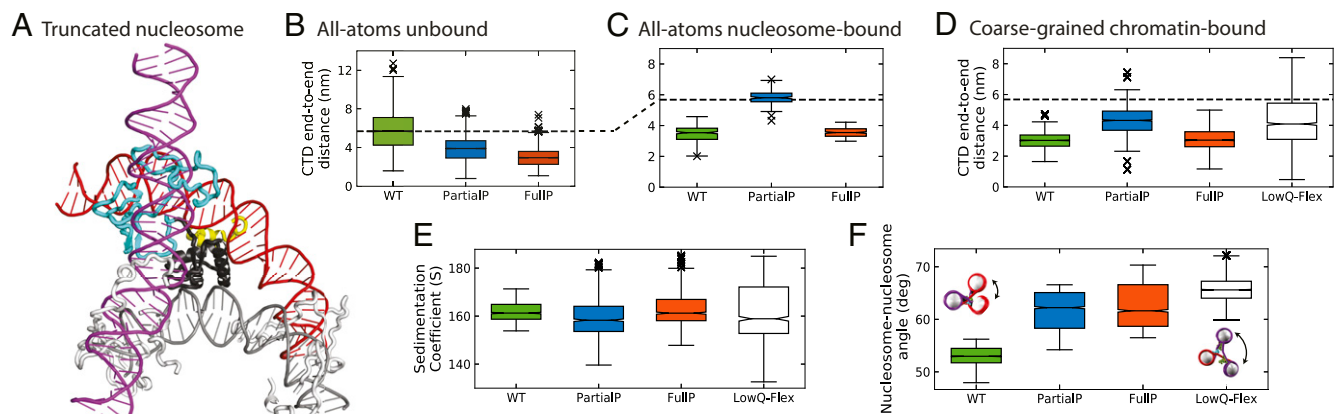


Fig. 6. Modulation of H1 CTD flexibility and chromatin structure by phosphorylation and hypothetical CTD charge modifications. (A) Visualization of the truncated nucleosome system used to model the phosphorylated CTDs at an atomistic scale. The color scheme of the constituents matches those in Fig. 1, and the core histone tails are depicted in white. (B) $C\alpha$ end-to-end distances from atomistic REST2 simulations for the unbound CTD of H1 comparing the WT, partially phosphorylated (PartialIP) and full phosphorylated (FullIP) systems. Dashed lines are shown to ease comparison of the smaller ranges plotted for the bound and coarse-grained systems. (C) The same comparison as in B but for the atomistic REST2 simulations of the nucleosome-bound systems. (D) End-to-end distance of the coarse-grained CTD of H1 within 100-nucleosome coarse-grained chromatin systems (containing one H1 bound to each nucleosome). We compare the values for the WT, PartialIP, FullIP, and low-charge but highly flexible CTD (LowQ-Flex) models. (E) Sedimentation coefficients and (F) triplet angles (and illustrations of angles) of the same 100-nucleosome coarse-grained chromatin systems analyzed in D. Box plots for the coarse-grained systems were obtained by bootstrapping the results from 12 independent MC trajectories per case.

performed additional 100-nucleosome coarse-grained simulations for such cases (12 Monte Carlo trajectories per condition) with our multiscale parameters transformed. Accordingly, the fully phosphorylated case was described with a less flexible CTD model and 40% of the charge of the WT tail, while the partially phosphorylated CTD was modeled as a chain with similar flexibility to the WT tail but with 70% of its charge (Fig. 6D and *SI Appendix, Supporting Methods*). To further rationalize how simultaneous modulation of flexibility and charge of the CTD regulates chromatin structure, we considered a hypothetical charge reducing chemical modification of the CTD that, unlike phosphorylation, increases the flexibility of the CTD (here termed “LowQ-Flex”).

Our coarse-grained simulations show that CTD charge-reduction leads to higher structural heterogeneity of chromatin, as evidenced by the wider distributions of sedimentation coefficients, triplet angles, and chromatin end-to-end distances (Fig. 6E and F and *SI Appendix, Fig. S7*). Furthermore, decreasing the charge of the CTD increases significantly the ability of chromatin to form contacts at longer genomic distances, favoring hierarchical looping (10–13) (Fig. 7). That is, while chromatin with WT H1 does not exhibit internucleosome contacts at distances greater than 10 kb (50 nucleosomes), more than 15% of the configurations adopted by chromatin with our reduced-charge H1 CTD models contained contacts at those large internucleosome distances (Fig. 7A). Chromatin with fully phosphorylated H1 produces more compact conformations and further enhances hierarchical looping (10–13), mimicking metaphase chromatin (Fig. 7C), while partially phosphorylated chromatin transiently populates a wider distribution of structures, including less compact ones, mimicking interphase chromatin (Fig. 7B). Increased flexibility coupled to charge reduction led to even higher structural heterogeneity of chromatin, increasing higher-order contacts and polymorphism (17) slightly more (Fig. 7A, LowQ-Flex).

Discussion

Our multiscale modeling investigation characterizes the statistical ensembles of the H1 protein when bound to the nucleosome at atomistic resolution and the implications of such atomistic behavior in large-scale chromatin organization at coarse-grained nucleosome resolution. Previous mesoscale modeling investigations have demonstrated that chromatin structure is regulated by

the cooperation of many factors, such as the DNA linker length (4) and its irregularity (17), the presence of acetylated residues (3), H1 binding (58) and density (4, 25, 40), the H1 asymmetry (26), and the cross-talk between many factors (12, 26). The related H1 CTD disorder explains experimental findings on chromosome asymmetry and provides the atomistic origins.

Our enhanced-sampling atomistic studies reveal that the CTD remains flexible and highly disordered when bound to a 211-bp nucleosome. This is consistent with recent breakthrough experiments showing that the H1 CTD is also disordered when bound to either free DNA (24) or the nuclear chaperon prothymosin α —a negatively charged and disordered protein (38). Despite its disorder, the CTD adopts a compact conformation, in agreement with NMR data (32), FRET (39, 59), and cryo-EM (34), and can be partitioned into four flexible lysine-rich loop regions that enable frequent fluctuating interactions between the CTD and both DNA arms in favor of DNA-DNA bridging. By remaining flexible but compact when bound to the nucleosome, the disordered CTD simultaneously brings DNA linkers into spatial proximity and enables enhanced DNA linker fluctuations.

A disordered H1 favors an asymmetric DNA stem with DNA linkers that curve and crisscross the dyad axis unevenly. Notably, loss of the two-fold symmetry is consistent with recent cryo-EM data for a 197-bp nucleosome (34) and our previous coarse-grained work (40). This loss of symmetry can be directly explained by differences in flexibility and conformations of the three H1 domains and the clear patterns of preferential interactions that they have for different DNA regions. While screening of the DNA-DNA electrostatic repulsion from the nucleosome edge to the DNA-DNA crossing point is mainly enabled by the more rigid GD and NTD (the latter having undergone a disorder-to-order transition upon DNA binding), screening at the crossing point and beyond is exclusively contributed by the flexible and disordered CTD. An important result of our work is that, by conferring a dynamic and asymmetric nature to the chromatin repeating unit, H1 CTD disorder favors looping and long-range interactions (10–13, 17) that are crucial for genome regulation. That is, increasing the asymmetry and flexibility of the CTD enhances the structural diversity of chromatin, promoting both compact structures with more prominent long-range loops and loose structures. A similar competition between compact looped structures versus loose conformations

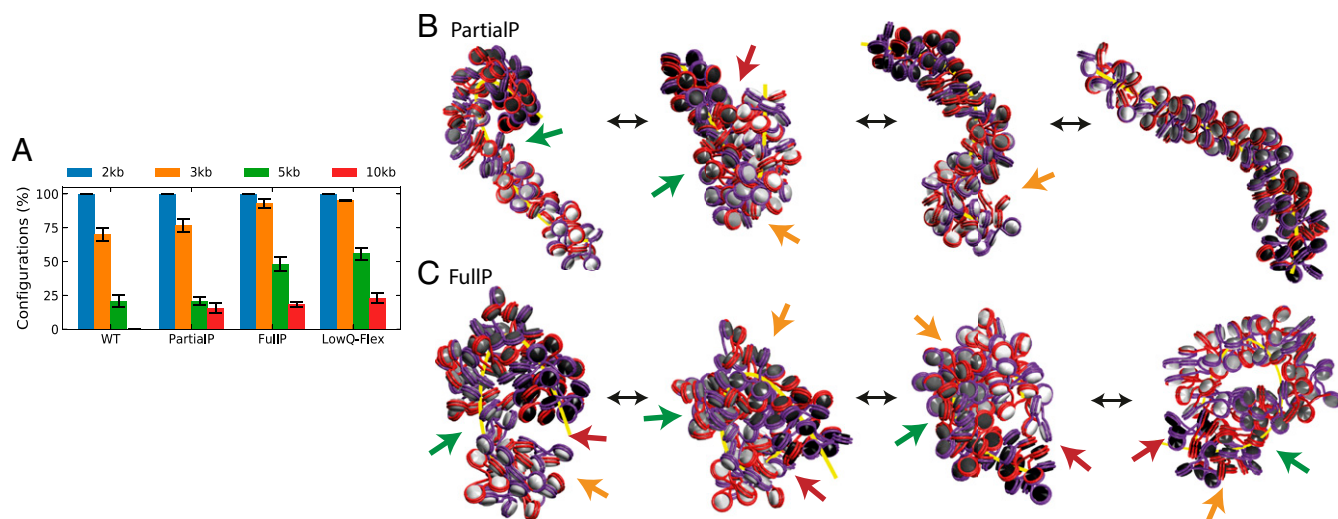


Fig. 7. Modulation of chromatin hierarchical looping by CTD chemical modifications. (A) Percentage of configurations with short-range (2 kb) and long-range contacts at 3, 5, and 10 kb with error bars representing 95% confidence intervals obtained by bootstrapping the results from the independent simulations. (B and C) Space filling models illustrating configurations with different long-range contacts for 100-nucleosome arrays with H1 bound with different degrees of phosphorylation. The probability of loop formation as a function of loop size for these systems is also quantified in *SI Appendix, Fig. S9*. This shows that CTD charge reduction is required for chromatin to be flexible enough to exhibit a nonzero probability of forming full loops (i.e., in which the first and last nucleosome, separated by 20 kb, contact each other). Color coding for chromatin images and arrows is as in Figs. 1 and 5.

has been recently noted in mesoscale simulations of chromatin that consider irregular H1 variants that bind nucleosomes in different on-dyad vs. off-dyad modes (26).

The degree of flexibility of the CTD within the nucleosome can be directly altered by the introduction of histone post-translational modifications, specifically different degrees of serine and threonine phosphorylation. We suggest that other epigenetic marks that change the flexibility of the CTD are expected to modulate directly the structure of chromatin. Moderate CTD charge reduction and increased CTD flexibility (mimicking partial phosphorylation) yield less condensed and more heterogeneous chromatin, while a stronger charge reduction coupled to decreased CTD flexibility (mimicking hyperphosphorylation) produces more compact chromatin conformations and a higher probability of establishing long-range contacts. These effects are consistent with partial phosphorylation of H1 correlating with chromatin decondensation in interphase chromosomes (13, 60, 61) and decreasing the capacity of H1 to compact free DNA with respect to WT (62). It is also consistent with the observation that hyperphosphorylation of H1, which is present during mitotic chromosome condensation (63), compacts free DNA in the same way as WT H1 (62). We propose that phosphorylation of serines and threonines of H1 is among the selected set of epigenetic changes, along with H4 lysine 16 acetylation (3), that can directly modulate chromatin structure. In addition, we suggest that charge-reducing chemical modifications that instead induce increased CTD flexibility could intensify significantly chromatin's fluid behavior and its ability to form longer-range contacts even further.

Conclusion

Our multiscale study demonstrates that nucleosome-bound H1 is highly disordered and that such disorder affects chromatin organization significantly. H1 disorder breaks up the symmetry of the nucleosome, inducing irregular DNA linker bending and enhancing DNA fluctuations. Nucleosome asymmetry and DNA fluctuations

in turn favor chromatin conformations that are simultaneously compact and hierarchically looped (10–13). Our work also puts forward control of the charge and flexibility of the H1 CTD as an additional mechanism for the regulation of chromatin looping, with lower CTD charge favoring looping. Taken together, our multiscale study bridging the atomic level with a mesoscale level of chromatin sheds light on a long-standing question concerning the structure and dynamics of H1 within the nucleosome, promotes the notion of H1-bound nucleosomes as asymmetric and flexible units, and suggests implications of H1 disorder on large-scale organization of chromatin.

Methods

All of the relevant methods are described in detail in *SI Appendix*.

Data Availability. All relevant data is included in the main manuscript, the *SI Appendix*, and the University of Cambridge Data Repository (<https://doi.org/10.17863/CAM.49850>).

ACKNOWLEDGMENTS. This project received funding from the European Research Council under the European Union's Horizon 2020 Research and Innovation Programme (Grant 803326). R.C.-G. is an Advanced Fellow from the Winton Programme for the Physics of Sustainability. T.S. received funding from the NIH National Institute of General Medical Sciences Awards R01GM055264 and R35-GM122562 and from Phillip-Morris USA and Phillip-Morris International. S.E.F. acknowledges the Engineering and Physical Sciences Research Council (EPSRC) Centre for Doctoral Training in Computational Methods for Materials Science for funding under grant no. EP/L015552/1. This work was performed using resources provided by the Cambridge Tier-2 system operated by the University of Cambridge Research Computing Service (<https://www.hpc.cam.ac.uk/>) funded by EPSRC Tier-2 capital grant EP/P020259/1, by the Advanced Research Computing High End Resource (ARCHER) system at the UK National Supercomputing Service (Project e459), and by the Red Española de Supercomputación (Projects QCM-2018-3-0041 and QCM-2018-2-0037). G.P. was funded by Wellcome Trust Grant 099232/z/12/z. We thank Massimiliano Bonomi for invaluable help with our BE-MetaD simulations and Anna R. Panchenko and Alexey K. Shaytan for providing their code to align nucleosomes to the dyad plane.

1. K. Luger, A. W. Mäder, R. K. Richmond, D. F. Sargent, T. J. Richmond, Crystal structure of the nucleosome core particle at 2.8 Å resolution. *Nature* **389**, 251–260 (1997).
2. T. Schlick, J. Hayes, S. Grigoryev, Toward convergence of experimental studies and theoretical modeling of the chromatin fiber. *J. Biol. Chem.* **287**, 5183–5191 (2012).

3. R. Collepardo-Guevara et al., Chromatin unfolding by epigenetic modifications explained by dramatic impairment of internucleosome interactions: A multiscale computational study. *J. Am. Chem. Soc.* **137**, 10205–10215 (2015).
4. O. Perišić, R. Collepardo-Guevara, T. Schlick, Modeling studies of chromatin fiber structure as a function of DNA linker length. *J. Mol. Biol.* **403**, 777–802 (2010).

5. T. Schalch, S. Duda, D. F. Sargent, T. J. Richmond, X-ray structure of a tetranucleosome and its implications for the chromatin fibre. *Nature* **436**, 138–141 (2005).
6. F. Song *et al.*, Cryo-Em study of the chromatin fiber reveals a double helix twisted by tetranucleosomal units. *Science* **344**, 376–380 (2014).
7. M. Kruijthof *et al.*, Single-molecule force spectroscopy reveals a highly compliant helical folding for the 30-nm chromatin fiber. *Nat. Struct. Mol. Biol.* **16**, 534–540 (2009).
8. S. A. Grigoryev, G. Arya, S. Correll, C. L. Woodcock, T. Schlick, Evidence for heteromorphous chromatin fibers from analysis of nucleosome interactions. *Proc. Natl. Acad. Sci. U.S.A.* **106**, 13317–13322 (2009).
9. K. Maeshima, R. Imai, S. Tamura, T. Nozaki, Chromatin as dynamic 10-nm fibers. *Chromosoma* **123**, 225–237 (2014).
10. G. D. Bascom, K. Y. Sanbonmatsu, T. Schlick, Mesoscale modeling reveals hierarchical looping of chromatin fibers near gene regulatory elements. *J. Phys. Chem. B* **120**, 8642–8653 (2016).
11. G. Bascom, T. Schlick, Linking chromatin fibers to gene folding by hierarchical looping. *Biophys. J.* **112**, 434–445 (2017).
12. G. D. Bascom, C. G. Myers, T. Schlick, Mesoscale modeling reveals formation of an epigenetically driven HOXC gene hub. *Proc. Natl. Acad. Sci. U.S.A.* **116**, 4955–4962 (2019).
13. S. A. Grigoryev *et al.*, Hierarchical looping of zigzag nucleosome chains in metaphase chromosomes. *Proc. Natl. Acad. Sci. U.S.A.* **113**, 1238–1243 (2016).
14. Y. Joti *et al.*, Chromosomes without a 30-nm chromatin fiber. *Nucleus* **3**, 404–410 (2012).
15. H. D. Ou *et al.*, ChromEMT: Visualizing 3D chromatin structure and compaction in interphase and mitotic cells. *Science* **357**, eaag0025 (2017).
16. K. Maeshima, S. Ide, K. Hibino, M. Sasai, Liquid-like behavior of chromatin. *Curr. Opin. Genet. Dev.* **37**, 36–45 (2016).
17. R. Collepardo-Guevara, T. Schlick, Chromatin fiber polymorphism triggered by variations of DNA linker lengths. *Proc. Natl. Acad. Sci. U.S.A.* **111**, 8061–8066 (2014).
18. M. A. Ricci, C. Manzo, M. F. Garcia-Parajo, M. Lakadamyali, M. P. Cosma, Chromatin fibers are formed by heterogeneous groups of nucleosomes in vivo. *Cell* **160**, 1145–1158 (2015).
19. A. V. Onufriev, H. Schiessel, The nucleosome: From structure to function through physics. *Curr. Opin. Struct. Biol.* **56**, 119–130 (2019).
20. J. B. Boulé, J. Mozziconacci, C. Lavelle, The polymorphisms of the chromatin fiber. *J. Phys. Condens. Matter* **27**, 033101 (2015).
21. G. Arya, T. Schlick, Role of histone tails in chromatin folding revealed by a mesoscopic oligonucleosome model. *Proc. Natl. Acad. Sci. U.S.A.* **103**, 16236–16241 (2006).
22. G. Arya, T. Schlick, A tale of tails: How histone tails mediate chromatin compaction in different salt and linker histone environments. *J. Phys. Chem. A* **113**, 4045–4059 (2009).
23. E. M. Bradbury *et al.*, Studies on the role and mode of operation of the very-lysine-rich histone H1 (F1) in eukaryote chromatin. The conformation of histone H1. *Eur. J. Biochem.* **52**, 605–613 (1975).
24. A. L. Turner *et al.*, Highly disordered histone H1-DNA model complexes and their condensates. *Proc. Natl. Acad. Sci. U.S.A.* **115**, 11964–11969 (2018).
25. O. Perišić, T. Schlick, Dependence of the linker histone and chromatin condensation on the nucleosome environment. *J. Phys. Chem. B* **121**, 7823–7832 (2017).
26. O. Perišić, S. Portillo-Ledesma, T. Schlick, Sensitive effect of linker histone binding mode and subtype on chromatin condensation. *Nucleic Acids Res.* **47**, 4948–4957 (2019).
27. E. Y. Popova *et al.*, Developmentally regulated linker histone H1c promotes heterochromatin condensation and mediates structural integrity of rod photoreceptors in mouse retina. *J. Biol. Chem.* **288**, 17895–17907 (2013).
28. J. Bednar *et al.*, Nucleosomes, linker DNA, and linker histone form a unique structural motif that directs the higher-order folding and compaction of chromatin. *Proc. Natl. Acad. Sci. U.S.A.* **95**, 14173–14178 (1998).
29. A. Routh, S. Sandin, D. Rhodes, Nucleosome repeat length and linker histone stoichiometry determine chromatin fiber structure. *Proc. Natl. Acad. Sci. U.S.A.* **105**, 8872–8877 (2008).
30. C. L. Woodcock, S. A. Grigoryev, R. A. Horowitz, N. Whitaker, A chromatin folding model that incorporates linker variability generates fibers resembling the native structures. *Proc. Natl. Acad. Sci. U.S.A.* **90**, 9021–9025 (1993).
31. D. Pruss *et al.*, An asymmetric model for the nucleosome: A binding site for linker histones inside the DNA gyres. *Science* **274**, 614–617 (1996).
32. B. R. Zhou *et al.*, Structural insights into the histone H1-nucleosome complex. *Proc. Natl. Acad. Sci. U.S.A.* **110**, 19390–19395 (2013). Correction in: *Proc. Natl. Acad. Sci. U.S.A.* **111**, 1222 (2014).
33. B. R. Zhou *et al.*, Structural mechanisms of nucleosome recognition by linker histones. *Mol. Cell* **59**, 628–638 (2015).
34. J. Bednar *et al.*, Structure and dynamics of a 197 bp nucleosome in complex with linker histone H1. *Mol. Cell* **66**, 384–397.e8 (2017).
35. M. A. Öztürk, G. V. Pachov, R. C. Wade, V. Cojocaru, Conformational selection and dynamic adaptation upon linker histone binding to the nucleosome. *Nucleic Acids Res.* **44**, 6599–6613 (2016).
36. A. Luque, G. Ozer, T. Schlick, Correlation among DNA linker length, linker histone concentration, and histone tails in chromatin. *Biophys. J.* **110**, 2309–2319 (2016).
37. A. Roque, I. Ponte, P. Suau, Role of charge neutralization in the folding of the carboxy-terminal domain of histone H1. *J. Phys. Chem. B* **113**, 12061–12066 (2009).
38. A. Borgia *et al.*, Extreme disorder in an ultrahigh-affinity protein complex. *Nature* **555**, 61–66 (2018).
39. H. Fang, S. Wei, T. H. Lee, J. J. Hayes, Chromatin structure-dependent conformations of the H1 CTD. *Nucleic Acids Res.* **44**, 9131–9141 (2016).
40. A. Luque, R. Collepardo-Guevara, S. Grigoryev, T. Schlick, Dynamic condensation of linker histone C-terminal domain regulates chromatin structure. *Nucleic Acids Res.* **42**, 7553–7560 (2014).
41. V. Ramakrishnan, J. T. Finch, V. Graziano, P. L. Lee, R. M. Sweet, Crystal structure of globular domain of histone H5 and its implications for nucleosome binding. *Nature* **362**, 219–223 (1993).
42. K. Lindorff-Larsen *et al.*, Improved side-chain torsion potentials for the Amber ff99SB protein force field. *Proteins* **78**, 1950–1958 (2010).
43. A. Pérez *et al.*, Refinement of the AMBER force field for nucleic acids: Improving the description of alpha/gamma conformers. *Biophys. J.* **92**, 3817–3829 (2007).
44. W. L. Jorgensen, J. Chandrasekhar, J. D. Madura, R. W. Impey, M. L. Klein, Comparison of simple potential functions for simulating liquid water. *J. Chem. Phys.* **79**, 926 (1983).
45. R. B. Best, W. Zheng, J. Mittal, Correction to balanced protein-water interactions improve properties of disordered proteins and non-specific protein association. *J. Chem. Theory Comput.* **11**, 1978 (2015).
46. J. L. F. Abascal, C. Vega, A general purpose model for the condensed phases of water: TIP4P/2005. *J. Chem. Phys.* **123**, 234505 (2005).
47. J. Huang *et al.*, CHARMM36m: An improved force field for folded and intrinsically disordered proteins. *Nat. Methods* **14**, 71–73 (2017).
48. K. Hart *et al.*, Optimization of the CHARMM additive force field for DNA: Improved treatment of the BI/BI conformational equilibrium. *J. Chem. Theory Comput.* **8**, 348–362 (2012).
49. D. A. Beard, T. Schlick, Modeling salt-mediated electrostatics of macromolecules: The discrete surface charge optimization algorithm and its application to the nucleosome. *Biopolymers* **58**, 106–115 (2001).
50. A. K. Shaytan *et al.*, Coupling between histone conformations and DNA geometry in nucleosomes on a microsecond timescale: Atomistic insights into nucleosome functions. *J. Mol. Biol.* **428**, 221–237 (2016).
51. T. L. Caterino, H. Fang, J. J. Hayes, Nucleosome linker DNA contacts and induces specific folding of the intrinsically disordered H1 carboxyl-terminal domain. *Mol. Cell. Biol.* **31**, 2341–2348 (2011).
52. A. Roque, I. Iloro, I. Ponte, J. L. R. Arrondo, P. Suau, DNA-induced secondary structure of the carboxyl-terminal domain of histone H1. *J. Biol. Chem.* **280**, 32141–32147 (2005).
53. K. Maeshima, S. Hihara, M. Eltsov, Chromatin structure: Does the 30-nm fibre exist in vivo? *Curr. Opin. Cell Biol.* **22**, 291–297 (2010).
54. K. Bystrycky, P. Heun, L. Gehlen, J. Langowski, S. M. Gasser, Long-range compaction and flexibility of interphase chromatin in budding yeast analyzed by high-resolution imaging techniques. *Proc. Natl. Acad. Sci. U.S.A.* **101**, 16495–16500 (2004).
55. D. T. Brown, B. T. Alexander, D. B. Sittman, Differential effect of H1 variant over-expression on cell cycle progression and gene expression. *Nucleic Acids Res.* **24**, 486–493 (1996).
56. N. Happel, D. Doenecke, Histone H1 and its isoforms: Contribution to chromatin structure and function. *Gene* **431**, 1–12.
57. R. A. Swank *et al.*, Four distinct cyclin-dependent kinases phosphorylate histone H1 at all of its growth-related phosphorylation sites. *Biochemistry* **36**, 13761–13768 (1997).
58. R. Collepardo-Guevara, T. Schlick, Crucial role of dynamic linker histone binding and divalent ions for DNA accessibility and gene regulation revealed by mesoscale modeling of oligonucleosomes. *Nucleic Acids Res.* **40**, 8803–8817 (2012).
59. H. Fang, D. J. Clark, J. J. Hayes, DNA and nucleosomes direct distinct folding of a linker histone H1 C-terminal domain. *Nucleic Acids Res.* **40**, 1475–1484 (2012).
60. A. Contreras *et al.*, The dynamic mobility of histone H1 is regulated by cyclin/CDK phosphorylation. *Mol. Cell. Biol.* **23**, 8626–8636 (2003).
61. R. Lopez *et al.*, Linker histone partial phosphorylation: Effects on secondary structure and chromatin condensation. *Nucleic Acids Res.* **43**, 4463–4476 (2015).
62. A. Roque, I. Ponte, J. L. R. Arrondo, P. Suau, Phosphorylation of the carboxy-terminal domain of histone H1: Effects on secondary structure and DNA condensation. *Nucleic Acids Res.* **36**, 4719–4726 (2008).
63. J. P. H. Th'ng, X. W. Guo, R. A. Swank, H. A. Crissman, E. M. Bradbury, Inhibition of histone phosphorylation by staurosporine leads to chromosome decondensation. *J. Biol. Chem.* **269**, 9568–9573 (1994).
64. M. Rawiso, From intensity to structure in physical chemistry of polymers. *J. Phys. IV* **9**, 147–195 (1999).
65. J. E. Kohn *et al.*, Random-coil behavior and the dimensions of chemically unfolded proteins. *Proc. Natl. Acad. Sci. U.S.A.* **101**, 12491–12496 (2004). Correction in: *Proc. Natl. Acad. Sci. U.S.A.* **102**, 14475 (2005).